# Encapsulation of apatite particles for improvement in bone regeneration

L. M. RODRÍGUEZ-LORENZO, K. A. GROSS*
*School of Physics and Materials Engineering, Building 69, Monash University, VIC 3800, Australia*
*E-mail: karlis.gross@spme.monash.edu.au*

The layering of fluorapatite on hydroxyapatite bodies provides a means of decreasing the solubility of hydroxyapatite, providing fluoride for possible stimulation of bone formation and delaying the release of calcium and phosphate from the more soluble hydroxyapatite. The purpose of this work was to encapsulate hydroxyapatite particles with fluorapatite spanning a thickness more than several crystallites deep. A three-step procedure was employed. Hydroxyapatite powder was immersed in an electrolyte solution until an equilibrium was established between the solid and the dissolved calcium at pH 4.67 and 37 °C. Equilibrium was determined by measurement of dissolved calcium with a calcium-specific ion-specific electrode. A $5 \times 10^{-2}$ M ammonium fluoride added to the suspension resulted in a rapid decrease of both calcium and fluoride in the solution. Analysis with X-ray diffraction indicated that a fluoride rich layer containing calcium fluoride deposited onto the particle surface. Scanning electron microscopy revealed submicron spherical precipitate clusters on the hydroxyapatite particles. These clusters transformed to fluorapatite by soaking in a 0.1 M $K_2HPO_4$ solution at pH 8 and 70 °C. A total time of 10 h was necessary for complete transformation of $CaF_2$ into fluorapatite.


## Introduction

Biomedical applications of fluoride-enriched hydroxyapatites has been targeted for both the dental and orthopaedic areas. Most attention has been accented towards the dental area realizing that prevention of caries is possible with a fluoride enriched hydroxyapatite [1, 2]. Initial investigations have focused on the synthesis of chemically modified apatites, where the chemical enrichment occurs homogeneously within submicron crystallites [3–5]. Since chemical enrichment of apatites can lead to a modification of physico-chemical properties, this chemical modification can be confined to the outer surface of the precipitated crystals. The type of proposed fluoride enrichment has included a single fluorapatite layer on the outside of a crystal [3], a multilayered configuration with increasing fluoride content towards the outside of the crystal [6], and a functionally graded layer with a continuous increase in fluoride content directed towards the outside of the crystal [7]. The most successful of these treatments involved the production of a stepped fluoride concentration within the crystal. While these procedures apply a chemical enrichment of apatites at the nanometer level, no work has been performed with thicker fluoride rich layers on larger apatite bodies consisting of a collection of fluorapatite crystals on a hydroxyapatite body, which is more relevant for orthopaedic applications.

Fluoride compounds remain amongst the most potent agents promoting bone formation and consequently species, such as fluorapatites and sodium fluoride have been investigated as possible biomaterials for osseous regeneration [8]. Nevertheless, the use of soluble compounds remains controversial since it has been observed clinically that an increase in bone formation is not necessary accompanied by a reduction in bone fractures [9]. The explanation given is related with a reduction in quality of the newly bone formed. *In vivo* experiments have revealed that short-term exposures to fluoride lead to greater bone densities but longer exposures results in periosteal bone formation and calcification of ligaments and tendons [10]. Consequently, if a fluoride containing material is used for bone healing and regeneration, it seems important to avoid excessive fluoride exposure. This situation can be achieved with a functionally graded material formed by an external fluoride rich layer that can initially stimulate bone growth followed by a supply of calcium and phosphate from hydroxyapatite in the core of a particle.

A layer of fluorapatite (FAp) can be grown on a hydroxyapatite particle through the following reaction:

$$Ca_{10}(PO_4)_6(OH)_2 + 2F^- \rightarrow Ca_{10}(PO_4)_6F_2 + 2OH^- \quad (1)$$

as shown in a previous paper [11]. However, the

*Author to whom all correspondence should be addressed.

thickness of the layer that can be obtained using this reaction is not much larger than 10 nm. When the purpose is to obtain a layer thicker than the mentioned value, a second approach must be employed. This is possible by the formation of a calcium rich compound initially by the following reaction:

$$Ca_{10}(PO_4)_6(OH)_2 + 20F^- \rightarrow 10CaF_2 + 6PO_4^{3-} + 2OH^- \quad (2)$$

Calcium fluoride can then be transformed into fluorapatite through one of the following reactions [12]:

$$10CaF_2 + 6H_2PO_4^- \rightarrow Ca_{10}(PO_4)_6F_2 + 18F^- + 12H^+ \quad (3)$$

$$10CaF_2 + 6HPO_4^{2-} \rightarrow Ca_{10}(PO_4)_6F_2 + 18F^- + 6H^+ \quad (4)$$

Reaction 2 will prevail over Reaction 1 for high activities of $F^-$ while high $PO_4^{3-}$ activities favors the stability of FAp in the solution as can be deduced from [13–15]:

$$(Ca^{2+})(F^-)^2 = K_{sp}(CaF_2) = 2.8 \times 10^{-11} \quad (5)$$

$$(Ca^{2+})^5(PO_4^{3-})^3(F^-) = K_{sp}(FAp) = 2.5 \times 10^{-60} \quad (6)$$

$$\log (F^-) = 0.33 \log (PO_4^{3-}) + 0.76 \quad (7)$$

The purpose of the present work is to grow a thick layer of fluorapatite on the surface of hydroxyapatite particles. A procedure based on Reaction 2 and subsequent reactions has been followed.

## Experimental

A commercial hydroxyapatite powder, Camceram (supplied by CAM Implants b.v., The Netherlands) was used for these experiments. Phase purity was verified by X-ray diffraction. XRD patterns were obtained using a Rigaku Geigerflex diffractometer (Rigaku, Japan) with copper $K_\alpha$ radiation generated at 22.5 mA and 40 kV passing through a 0.3° receiver and 0.5° divergence slit. A step scan with 10 seconds per step and a step size of 0.02° were selected over a two theta range of 10–90. Crystallite size was determined in the $\langle 1\,0\,0 \rangle$ and $\langle 0\,0\,1 \rangle$ direction by using the Scherrer equation [16]. Specific surface area $(A)$ was determined using the BET method [17]. The five-point method with nitrogen as gas filler was performed using a Micromeritics Gemini 2360 (Norcross, GA, USA) to determine the specific surface area. Particle size distribution was determined in a Saturn Digisizer 5200 (Micromeritics, Norcross, GA, USA) that employs a laser diffraction method.

Size and morphology of the materials were studied with a Hitachi S570 scanning electron microscopy (SEM) (Tokyo, Japan) at 10 kV and a working distance of 10 mm.

A multistep procedure was employed to produce hydroxyapatite particles encapsulated in a layer of fluorapatite. For the first step, 5 g of Camceram were soaked in 250 ml of a $2 \times 10^{-1}$ M $KNO_3$ solution ($KNO_3$ was used as supporting electrolyte) in a polyethylene reaction vessel at pH 4.67 and 37 °C. The suspensions were mechanically stirred at 800 r.p.m. and the powder was allowed to reach an equilibrium with the liquid. The pH of the solution was set and maintained by adding a 0.005 M acetic/acetate buffer (pH 4.67) with a pH stat (Titrino 736, Metrohm, Switzerland). The calcium ion concentration was monitored with a calcium ion selective electrode connected to a PHM 250 ion analyzer (Radiometer, Copenhagen, Denmark). After 90 min of equilibration, a $5 \times 10^{-2}$ M ammonium fluoride solution was added to the suspension. In this step, calcium and fluoride were monitored with the corresponding ion selective electrodes during stirring over a period of 3 h. Particles were collected by filtering through a 20 μm stainless steel sieve with the aqueous solution from the reaction. Residual fluoride remaining in the solution was determined with the same fluoride ion selective electrode described previously. Finally, the powders were dried at 80 °C.

Powders were then soaked in a 0.1 M $K_2HPO_4$ solution at pH 8 and 70 °C for different times. Fluoride ion content of each powder was determined with the solid state fluoride ion selective electrode following the method outlined by Singer and Armstrong [18]. The resulting powder was analyzed as described previously for the starting material. An energy dispersive X-ray analysis (EDXA) was performed with a Jeol JSM 840A (Tokyo, Japan) SEM on the polished sections for the fluoride ion distribution on the particle surface.

## Results and discussion

The secondary electron image of the supplied powder displays 20–80 μm rounded microspheres that contains densely packed fine crystallites (Fig. 1). The X-ray diffraction pattern, displayed in the inset of Fig. 1,

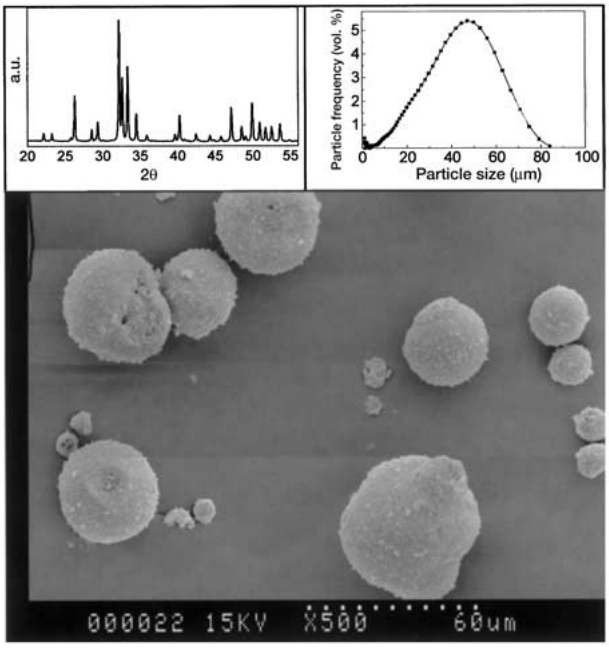


*Figure 1* Scanning electron micrograph of the powder. Left inset, XRD pattern of the same material. Right inset, particle size distribution.

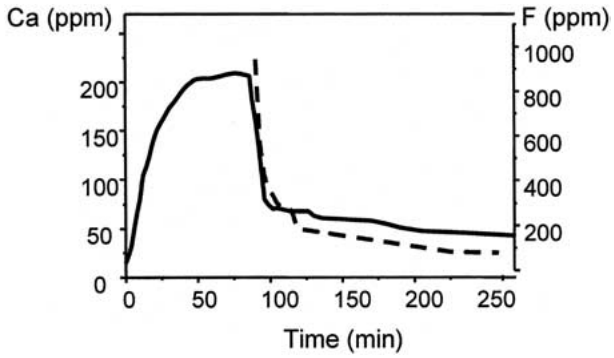


*Figure 2* Ca (solid line) and F (dotted line) in solution during the first two steps of the procedure.

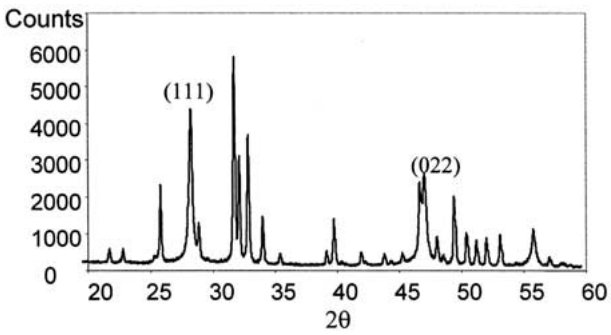


*Figure 3* X-ray diffraction pattern of the powder collected after the second step.

shows that the material is made of a single phase hydroxyapatite [19]. No evidence of peaks corresponding to a secondary phase could be found. The application of the Scherrer method to the diffraction pattern yields a crystal size of 128 nm in the $\langle 1\,0\,0 \rangle$ direction and 215 nm in the $\langle 0\,0\,1 \rangle$ direction. The specific surface area of the powder calculated by the BET method is $7\,m^2/g$. Particle size shows a monomodal distribution with a mean particle size of 45 µm in a size range between 10 and 80 µm. The smaller particles displayed in the particle size distribution of Fig. 1 are also noted in the secondary electron image.

When the powder is soaked in a $KNO_3$ solution, partial dissolution occurs until an equilibrium is reached. This step has been monitored with a calcium ion electrode as shown in Fig. 2. No calcium is detected in the initial solution but calcium is eluted to the medium after powder immersion and detected with the electrode indicating dissolution of the hydroxyapatite. Continuous dissolution occurs until 50 min, the time at which the calcium concentration in the medium becomes constant, indicating an equilibrium between the powder and the solution. Hydroxyapatite does not dissolve any further and this is supported by no further calcium ion increase in solution up to a period of 90 min. The reaction was conducted in a $KNO_3$ solution to maintain a constant ionic strength that produces reliable measurement with the electrode. The dissolution of hydroxyapatite is accompanied by an increase in the pH which is re-established with an acetic/acetate buffer to maintain constant pH conditions.

The second step of the procedure involves adding an ammonium fluoride solution. The fluoride concentration utilized has been chosen to ensure that Reaction 2 prevails over Reaction 1. Calcium and fluoride have been monitored along this step of the procedure. Results are displayed in Fig. 2. A marked decrease in calcium concentration in solution occurs upon addition of the fluoride, followed by a slow but continuous decrease with time. The amount of fluoride in solution decreases rapidly during the first minutes of the experiment, in a similar trend to the decrease in calcium concentration, followed by a period of continuous, but slower decrease. The evolution of the concentration of these ions in solution is compatible with the precipitation of $CaF_2$.

After 270 min, the powder was collected, dried and analyzed. The X-ray diffraction pattern of the collected powder is displayed in Fig. 3 showing the appearance of two diffraction maxima that have been assigned to $CaF_2$ [20]. The microsphere surface texture has also changed from the finer crystallites observed in the original powder. Particles are now covered by spherical crystalline precipitate clusters and an analysis by EDXA shows that this is a fluoride rich layer, Fig. 4. It can be deduced that a precipitation of $CaF_2$ has occurred during the second step and this precipitation has led to the encapsulation of the hydroxyapatite particles with a layer of calcium fluoride.

Powders with the calcium fluoride layer were then soaked in a phosphate solution. The linear function given by Equation 7 defines the regions in which $CaF_2$ and FAp are the most stable phases. The powder lies in the region where FAp is the most stable phase after addition of the phosphate as can be observed in Fig. 5. Therefore, a transformation of the $CaF_2$ layer can be expected. As stated in the literature [12], the mechanism of transformation involves the dissolution of the $CaF_2$ to provide calcium and fluoride ions and then these ions react with the phosphate of the medium to form the apatite crystals. Higher temperatures yield faster dissolution of the $CaF_2$ crystals in this mechanism. For this reason the third step of the procedure was conducted at 80 °C. The limitation

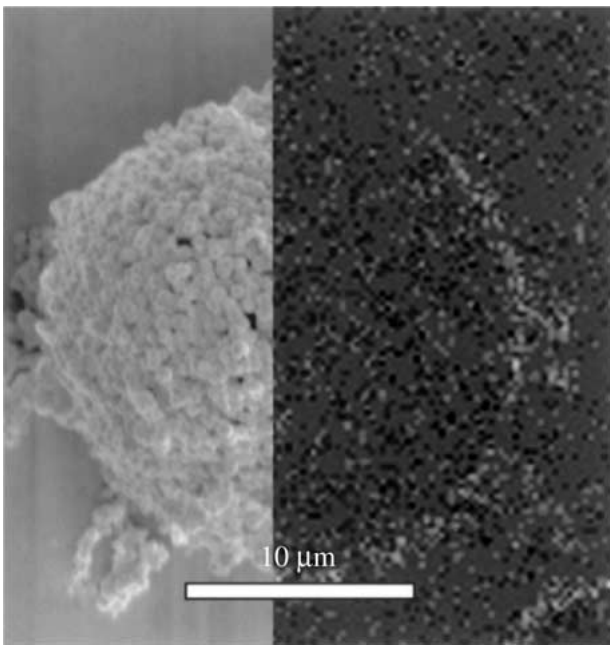


*Figure 4* Left, SEM picture of the powder after the second step. Right, EDXA analysis of the same powder, the white line representing the fluoride layer.

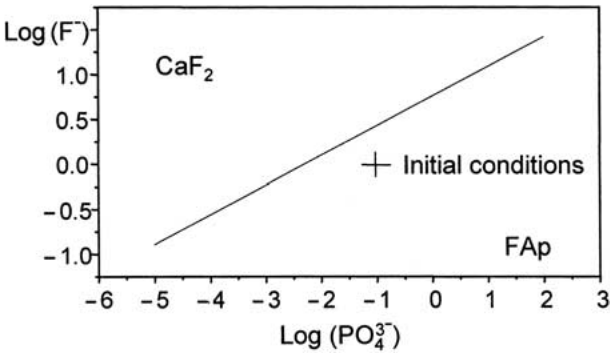


*Figure 5* Stability phase diagram of $CaF_2$ and FAp. Conditions selected for the third step are also displayed.

TABLE I Soaking time, fluoride content of solid and liquids ($F_{solid}$ and $F_{liquid}$) and ratio ($F_{liquid}/F_{solid}$) for the third step of the procedure

| Soaking time (hrs) | $F_{solid}$ (%) | $F_{liquid}(10^{-3}M)$ | $F_{liquid}/F_{solid}$ |
|---|---|---|---|
| 0 | 9.67 | — | — |
| 1 | 8.01 | 2.899 | 0.07 |
| 2 | 3.66 | 2.528 | 0.11 |
| 6 | 2.32 | 4.547 | 0.38 |
| 10 | 1.78 | 4.438 | 0.49 |

of working at this temperature has the shortcoming of not being able to monitor the ion concentration as done in the former steps described above. Consequently, the fluoride content has been analyzed for both the solid and liquids after defined times of reaction. Table I shows the fluoride content for both solid and liquids. According to Reactions 3 and 4, the amount of fluoride released to the medium is nine times the fluoride concentration that remains in the solid. This explains the decrease in fluoride content observed for the solid (Table I). If the reaction is complete, the fluoride liquid/solid ratio should then be nine; however, this value was never reached indicating that the reaction was continuing. The initial presence of FAp increases the ratio and could lead to a lower ratio as observed at longer immersion times. Total transformation can be confirmed by phase analysis of the phases as shown in Fig. 6. Increasing time of reaction yields a decrease in the intensities of the $CaF_2$ attributed peaks leading to a total disappearance after 10 h of soaking.

An explanation of the growth mechanism of FAp over

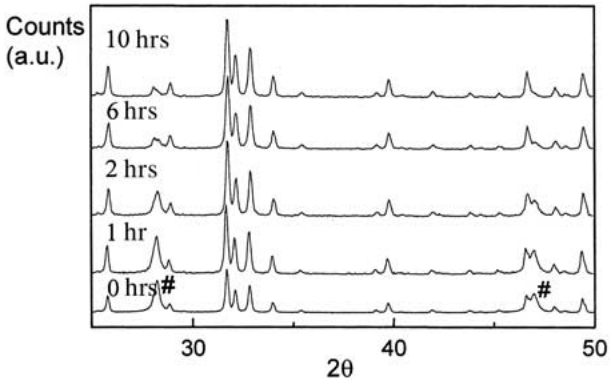


*Figure 6* XRD patterns of the powders recorded after the third step.

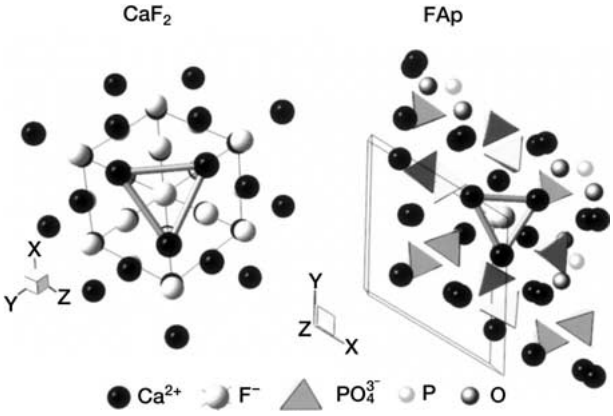


*Figure 7* Arrangement of ions at the plane $\langle 1\,1\,1 \rangle$ for $CaF_2$ and the perpendicular to the long axis for FAp showing analogous triangles of Ca ions.

$CaF_2$ requires the consideration of some crystallographic features. Calcium fluoride crystallizes in the cubic Fm-3m space group [14] and hydroxyapatite in the hexagonal $P6_3/m$ [21]. Calcium ions form a triangle of similar dimensions for each structure (3.861 Å for $CaF_2$ and 3.979 Å for FAp) with the center occupied by a fluoride ion. Fig. 7 shows a representation of the c face of the apatite structure and the $\langle 1\,1\,1 \rangle$ plane of the $CaF_2$ structure. The phosphate tetrahedron arrangement around this triangle for the apatite structure is similar to the arrangement of fluoride ions around the Ca triangle for the $CaF_2$ structure. It seems that the crystallographic unit formed by the triangles and surrounding atoms provides a nucleation site for the apatite growth that facilitates the transformation.

## Conclusions

Encapsulation of hydroxyapatite particles with a fluorapatite layer containing a collection of crystallites is possible by initial layering of calcium fluoride followed by transformation of a deposited calcium fluoride layer to fluorapatite. The transformation of calcium fluoride to fluorapatite requires immersion in a phosphate solution for a minimum of 10 h.

## Acknowledgments

Dr Gross was supported by an Australian Research Council Fellowship (grant no. F10017027) and Dr Rodriguez-Lorenzo with a supporting ARC Large grant (grant no. A10017174). The authors are grateful for the supply of Camceram powder used in this study by CAM Implants b.v.

## References

1. F. C. M. DRIESSENS, *Nature* **243** (1973) 420.
2. E. C. MORENO, M. KRESAK and R. T. ZAHRADNIK, *Caries Res.* **11** (1977) 142.
3. M. OKAZAKI, *Biomaterials* **13** (1992) 749.
4. L. J. JHA, S. M. BEST, J. C. KNOWLES, I. REHMAN, J. D. SANTOS and W. BONFIELD, *J. Mater. Sci.: Mater. Med.* **8** (1997) 185.
5. L. M. RODRÍGUEZ-LORENZO, J. N. HART and K. A. GROSS, *Biomaterials* **24** (2003) 3777.

6. M. OKAZAKI, Y. MIAKE, H. TOHDA, T. YANAGISAWA, T. MATSUMOTO and J. TAKAHASHI, *ibid*. **20** (1999) 1421.
7. M. OKAZAKI, Y. MIAKE, H. TOHDA, T. YANAGISAWA and J. TAKAHASHI, *ibid*. **20** (1999) 1303.
8. K. A. GROSS, J. HART and L. M. RODRÍGUEZ-LORENZO, *Key Eng. Mater*. **218–220** (2002) 165.
9. B. L. RIGGS, S. W. HODSON, W. M. O'FALLON, E. Y. S. CHAO, H. W. WAHNER, J. M. MUHS, S. L. CEDEL and L. J. MEETON, *N. Eng. J. Med*. **322** (1990) 802.
10. J. CAVERZASIO, G. PALMER and J. P. BONJOUR, *Bone* **22** (1998) 585.
11. L. M. RODRÍGUEZ-LORENZO and K. A. GROSS, *J. Amer. Ceram. Soc*. Accepted for publication (October 2002).
12. S. CHANDER, C. C. CHIAO and D. W. FUERSTENAU, *J. Dent. Res*. **61** (1982) 403.
13. L. C. CHOW and M. MARKOVIC, in ''Calcium Phosphate in Biological and Industrial Systems'', edited by Z. Amjad (Kluwer Academic Publishers, Boston, 1998) p. 67.
14. P. LEAMY, P. W. BROWN, K. TENHUISEN and C. RANDALL, *J. Biomed. Mater. Res*. **42** (1998) 458.
15. J. LIN, S. RAGHAVAN and D. W. FUERSTENEAU, *Colloids and Surfaces* **3** (1981) 357.
16. W. N. SCHERRER and R. JENKINS, *Adv. X-ray Analysis* **26** (1983) 141.
17. S. BRUNAUER, P. H. EMMETT and E. TELLER, *J. Am. Chem. Soc*. **60** (1938) 309.
18. L. SINGER and W. D. ARMSTRONG, *Anal. Chem*. **40** (1968) 613.
19. JCPDS no. 24-33 International Center for Diffraction Data 1999.
20. JCPDS no. 35-816 International Center for Diffraction Data 1999.
21. D. N. BATCHELDER and R. O. SIMMONS, *J. Chem. Phys*. **41** (1964) 2324.

*Received 18 March*
*and accepted 3 June 2003*